Grading Quality of Color Retinal Images to Assist Fundus Camera Operators

Sangeeta Biswas[†§], Johan Rohdin[†], Andrii Kavetskyi[†] and Martin Drahansky[†]
[†]*Centre of Excellence IT4Innovations, Faculty of Information Technology, Brno University of Technology*
Brno 61200, Czech Republic
[§]*Faculty of Engineering, University of Rajshahi, Rajshahi 6205, Bangladesh*
Email: {biswas, rohdin, ikavetskyi, drahan}@fit.vutbr.cz

***Abstract*—Suitable image quality is a prerequisite to ensure accurate diagnosis or person recognition by color retinal images. Many factors during image acquisition, transferring and storing can result in poor quality retinal images. Poor quality images not only increase the possibility of wrong diagnosis, false acceptance, or incorrect identification but also increase diagnosis or recognition time. Therefore, retinal image quality assessment has become an important research topic. In general, only one color channel (most of the time either *green* or *grayscale*) is used to assess the quality of retinal images ignoring the quality of other channels. However, all image channels carry complementary information. In this paper, we propose a quality assessment approach for a colored retinal image to assist a fundus camera operator to judge the image quality. In our approach, we analyze the histogram of pixel intensity and uniformity of illumination, as well as check the presence of two main anatomical structures, optic disc, and central retinal blood vessels, in all color channels (i.e., red, green and blue) as well as in grayscale format. We show the effectiveness of our approach by grading 3090 color retinal images of five publicly available retinal databases.**

***Index Terms*—color retinal image, quality assessment, convolutional neural network**

I. Introduction

The retina is a thin, semi-transparent, multi-layered, neural tissue that covers the two-thirds of the interior of each eye. It is anatomically and physiologically considered as an extension of our brain. It is mainly responsible for converting an incoming electromagnetic signal from the world outside of our eye into a neural signal and then handing over the neural signal to the optic nerve. The neural signal, relaying through optic nerves, forms images into the visual cortex of our brain, and therefore, we can have a sense of vision [3], [20]. Any kind of disturbance in the retina can have a negative effect on our vision. Severe pathology in the retina can even cause irreversible partial or complete vision loss. Besides vision, retina is also used for identifying individuals in order to control the access to highly confidential and secured environments. One reason is that central retinal blood vessels which are responsible for supplying oxygen and nutrients to the retina have a unique and almost lifetime permanent pattern. Therefore, retinal images are highly demanding by ophthalmologists, Computer-Aided Diagnostic systems (CADs), retinopathy researchers as well as by biometric researchers.

The color retinal images are widely used for detecting and monitoring the development of different kinds of pathology (such as diabetic retinopathy, age-related macular degeneration, glaucoma, retinitis pigmentosa, Stargardt disease, etc.,) in the retina, as well as for identifying individuals. Suitable image quality is prerequisite to ensure accurate diagnosis and individual identification by color retinal images. Many factors during image acquisition, transferring, and storing can result in poor quality retinal images. Factors can be the low experience level of the operator, operator's finger movement or shaking, low standard fundus cameras, subject's eye movement or blinking, curved structure of the retina, inadequate illumination, variation of pupil dilation, poor focus, compression-decompression techniques applied on images, transmission channels and so on. Poor quality retinal images not only increase the possibility of wrong diagnosis or recognition but also increase the diagnosing or recognition time. For example, blurred retinal images can hide retinopathy lesions so that a diseased retina could look like a normal retina [10]. Therefore ophthalmologists need to spend a long time to take any decision on a blurred image. Automatic CADs needs sophisticated algorithms considering different factors to improve image quality before taking automatic decision.

Our further observation is that poor quality images also force researchers to work on the green channel or grayscale format for their robustness, even though the other two channels carry complementary information. Many previous works on Retinal Image Quality Assessment (RIQA) (e.g., [4], [7], [10], [11], [17]–[19], [22], [25]) used only one color channel (either *green* or *grayscale*) to assess the quality of retinal images ignoring the quality of *blue* and *red* channels accepting as a fact that these channels could be noisy. Even though some researchers (e.g. [12], [21], [26], [30]) worked on three color channels, they used the three channels mainly for histogram-based features and not for all features they used to determine the quality of retinal images. An exception is the work done by Abdel-Hamid et al., [1]. Convolutional Neural Network (CNN) based RIQA approaches (e.g., [6], [28], [31]) used RGB retinal images as a whole without analysing the quality of each color channel separately.

As shown in Fig. 1, we can see the almost circular, colored foreground of a retina on a dark background in a color retinal image taken by a fundus camera. The foreground of the retina is covered by tree-structured Central Retinal Arteries (CRAs) and Central Retinal Veins (CRVs). The CRAs

2372-9198/20/$31.00 ©2020 IEEE
DOI 10.1109/CBMS49503.2020.00022

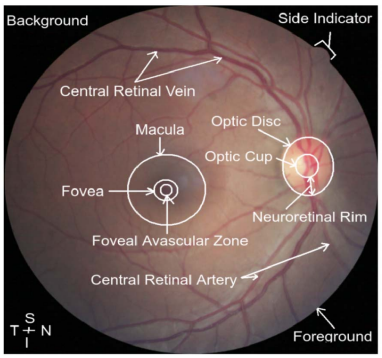

Fig. 1. Visibility of main anatomical structures in a color fundus photograph of a healthy right retina. Note that, the boundaries of the macula, fovea, OD, OC, NR are not accurately drawn.

and CRVs together form the Central Retinal Blood Vessels (CRBVs). Other anatomical structures such as the macula, fovea, Optic Disc (OD), Optic Cup (OC), Neuroretinal Rim (NR), are also visible in a color retinal image. Our assumption is that a good quality colored retinal image should have a foreground which is uniformly illuminated as well as clearly show at least the main anatomical structures (i.e., OD, macula, CRBVs, etc.,) of a retina, no matter whether it is displayed in a specific color channel (i.e., in the red, green or blue channel) or in the combination of three color channels (i.e., in grayscale format). However, during taking images, it is hard for the fundus camera operators to realize the quality of all anatomical structures in each channel in bare eyes. Therefore, we implement an approach that is a hybrid of generic and content based quality assessment approaches. We estimate the quality of a retinal image by analyzing its histogram of pixel intensity as well as checking the presence of its two main anatomical structures, OD and CRBVs in each color channel as well as in the grayscale format. In this paper, we limit ourselves to the two most dominant structures (i.e., OD and CRBVs) because of the lack of annotated data for other structures. In future work, we will consider more anatomical structures.

We believe our approach will help operators (no matter whether they are experienced ophthalmologists, ophthalmic nurses, or people having short training period to capture retinal images either for medical or research purposes) to decide whether they need to retake pictures so that subjects do not need to come back again. Our observation is that asking subjects to come back for retaking retinal images most of the time is not well accepted (especially when images are taken from the volunteers for research purposes).

II. Experimental Setup

We do all implementations using TensorFlow's Keras API 2.1.6-tf, OpenCV library, and Python. We use a standard PC with Intel(R) Core(TM) i9-9900K having 8 Cores and 32 GB memory, and with two NVIDIA GeForce GTX 1080 GPUs having 8 GB memory per GPU.

TABLE I
Data sets used in our experiments.

Data Set	Resolution	# Imgs.	Purpose
DRIVE [29]			
TestSet	584×768	20	$*$ Training set for UNet_BVs
TrainingSet	584×768	20	$*$ Validation set for UNet_BVs
HRF_DR [5]	3264×4928	45	$*$ Training set for UNet_BVs
STARE [14]	605×700	20	$*$ Training set for UNet_BVs
UoA-DR [2]	2056×2124	200	$*$ Training set for UNet_BVs $*$ Training, validation & test set for UNet_ODs
CHASE_DB1 [24]	960×999	28	$*$ Test set for UNet_BVs $*$ Quality assessment
FIRE [13]	2912×2912	268	
HRF_RIQA [17]			
	2592×3888	26	
	3456×5184	10	
Kaggle [8]			
SetA	3264×4928	1558	$*$ Quality assessment
Messidor [9]			
	960×1440	588	
	1488×2240	400	
	1536×2304	212	

In our experiments, we use in total nine publicly available data sets for different purposes (see Table I for details). Among the five data sets we use for quality assessment, only HRF_RIQA is mainly designed for retinal image quality assessment. The CHASE_DB1 is generally used for assessing blood vessel segmentation algorithms, whereas the FIRE data set is designed for studies on retinal image registration, the Messidor and Kaggle data sets are for the studies of diabetic retinopathy detection. There are in total $42,111$ pairs of left and right retinal images (i.e., $84,222$ images) having 27 types of resolutions in the Kaggle data set. We choose 1558 images with resolution 3264×4928 because the foreground of this resolution has complete circular shape. We name it as Kaggle_SetA data set.

Since the dark pixels of the background do not provide any necessary information, we crop the background so that the foreground can touch the boundary without losing any important pixels of the foreground. Because of different resolutions of different data sets, we re-size all images to 256×256 by bicubic interpolation. Except that, no other pre-processing is applied to any images. We get grayscale images using the default setting of the OpenCV library (i.e., $0.299 \times red\_channel + 0.587 \times green\_channel + 0.144 \times blue\_channel$).

In order to get masks for the OD and to segment CRBVs, we train a U shaped CNN (i.e., U-Net [27]) for each color channel (i.e., *red*, *green* and *blue* channel) as well as for the grayscale format. Therefore, in total, we train eight U-Nets. The U-Net is well-known (especially for medical image segmentation) for its requirement of very few images in the training phase. For example, in [27], only 30 images were used to train a U-Net which outperformed a sliding window CNN for the ISBI neuronal structures in EM stacks challenge 2012. All of our U-Nets have the same architecture as shown in Fig. 2. We set *mean-squared-error (MSE)* as the loss function;

RMSProp as the optimizer and $mini\_batch\_size = 16$. For all convolutional layers and transposed convolutional layers, we set $kernel\_size = 3$ and $kernel\_size = 2$, respectively. However, for both kinds of layers, we set $padding = same$ and $kernel\_initializer = he\_normal$. We set these parameters based on previous experience with the same architecture on a variety of tasks. We use 20 images of the DRIVE as the validation set when training the U-Nets targeting to segment CRBVs (i.e., UNet_BVs), and 20 images of the UoA_DR as the validation set when training the U-Nets targeting to segment OD (i.e., UNet_ODs). Using the validation set, we decide the $epoch\_no$ and control the $optimizer\_learning\_rate$. For all other settings, we use the default values of TensorFlow's Keras API 2.1.6-tf. During training, it takes on average 2.8 seconds and 1.8 seconds to complete one epoch of UNet_BVs and UNet_ODs, respectively, in our GPU based machine. On average, after completing 512 epochs and 86 epochs, we achieve the optimum UNet_BV and UNet_OD, respectively, per color channel (i.e., the lowest MSE for the validation set by our U-Nets). We use 28 images of the CHASE_DB1 and 28 images of UoA_DR as the test sets for UNet_BVs and UNet_ODs, respectively. For UNet_BVs, we achieve 0.0545, 0.0313, 0.0153, and 0.0300 as MSE for the grayscale, red, green and blue color channel of the test set, respectively. On the other hand, for UNet_ODs, we achieve 0.0220, 0.0033, 0.0058, and 0.0054 as MSE for the grayscale, red, green and blue color channels of the test set, respectively.

III. Steps for Quality Assessment

Fig. 3 shows the flow diagram of our approach to estimate the quality of an RGB colored retinal image (say, I_{retina}). We describe each step briefly in the next five subsections.

A. Generating Foreground Mask

An almost circular shaped I_{target} has some dark background area no matter how much background we crop out. In order to avoid the effect of the background pixels in our further estimation, the first and foremost task is to generate a foreground mask (FGM). Since the grayscale format is less affected by noise, overexposure or underexposure than the *red*, *green* or *blue* channels, generating FGM using the grayscale format is less error-prone than using other color channels. Therefore, we choose the grayscale format to generate the FGM. Otsu's segmentation algorithm [23] can be used to generate the FGM. However, for non-uniformly illuminated or noisy retinal images, generated FGM will be distorted. Therefore, instead of this algorithm, we follow a simple approach. At first, we detect edges using *Canny's edge detection* algorithm [15]. After that we find the contour points belonging to each edge. Then for each contour, we estimate the radius of the circle that minimally encloses that contour. Among the obtained circles, the largest one is selected as the border between foreground and background. We fill the area between the selected circle (e.g., the red-colored circle in Fig. 4 (d)) with white pixels and generate the FGM (e.g., Fig. 4 (e)). The generated FGM is slightly bigger than the actual foreground if there is the *side indicator* (Case-2 of Fig. 4 (f)). Fixing this erroneous part is our future task. We use the functions of the OpenCV library for this part.

B. Skewness Based Score Generation

A simple histogram of intensity values of any channel reveals whether that channel is overexposed or underexposed or whether any specific intensity is dominating or not. If a histogram is leaned to the right side, it means that the channel is overexposed, whereas if it is leaned to the left side, it means that the channel is underexposed (see Fig. 5). The histogram of a good-quality channel will not be leaned to any specific side. The skewness of a histogram helps us measure leaning tendency. The lower the skewness value, the less biased a histogram. We assign $\mid (skewness) \mid^{-1}$ as skewness based score to a channel. Summing up all skewness based scores for all channels, we decide the skewness based score (say, *SkewQS*) for I_{target}. The value of *SkewQS* remains in the range $0 - 4$ for I_{target}.

C. Uniformity Based Score Generation

Otsu's algorithm [23] is a widely used thresholding based segmentation algorithm. This method selects an optimal threshold value automatically from a gray level histogram and uses to segment different parts of an image. In the simplest case, it is used to segment the foreground of an image from its background. However, this widely used segmentation algorithm fails to produce accurate segmentation results for non-uniform illuminated images [16]. Our assumption is that a good-quality channel of I_{target} should be uniformly illuminated. So, using Otsu's algorithm if we get a partial foreground for a channel, then that is a sign of a low-quality channel. Therefore, We can assign a quality score to each channel depending on how much area of the foreground we can get by Otsu's algorithm comparing to the FGM. Summing up all channels' scores we estimate a uniformity based score (say, *Uniformity*) for I_{target}. When there is a side indicator in a channel, then maybe we would get slightly smaller value than 1, even though we can segment the complete foreground.

D. Density of CRBVs Based Score Generation

At first, we binarize the manually segmented CRBVs and FGMs of the 40 images of the DRIVE data set and the 45 images of HRF_DR data set using Otsu's segmentation algorithm. Then we estimate the average blood vessel density (say, α_{dev}) in the area covered by the FGMs. After that, we predict segmented CRBVs for each channel of I_{target} by using channel-specific UNet_BV. Using the same process as we do for estimating α_{dev}, we estimate the blood vessel density (say, α_{target}) for each channel of I_{target}. Dividing α_{target} by α_{dev} we estimate score for that channel (see Fig. 6). Summing up all the scores of four channels, we estimate scores for I_{target}. The blood vessel based score for a specific channel can be in the range $0 - \beta$, where β is any positive number. Therefore, blood vessel density based score for I_{target} can be more than 4. We notice that β remains below 2 in the experiments.

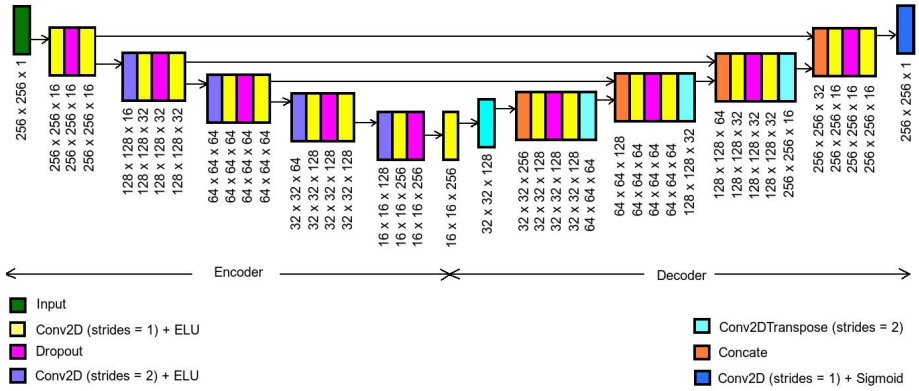

Fig. 2. The architecture of U-Net used to segment OD and CRBVs.

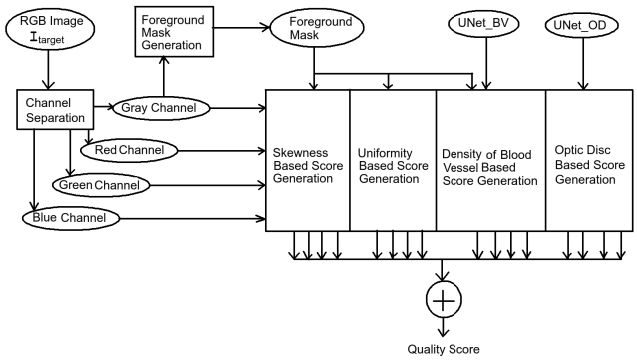

Fig. 3. A flow diagram of our approach to assess the quality of a retinal image.

E. Optic Disc Based Score Generation

At first, using the UoA_DR data set, we estimate the minimum radius and maximum radius (say, θ_{min} and θ_{max}) of the enclosing circle of a possible OD. Then we predict an OD mask for each channel of a retinal image by using channel-specific UNet_OD. Then we binarize the OD mask using Otsu's segmentation algorithm. After that, using θ_{min} and θ_{max} as thresholds, we count the number of possible ODs in the OD mask. If no OD is counted, that channel scores 0, whereas it scores 1 when only one OD is counted. If multiple ODs are counted, it is possible that the channel is noisy or has some pathology such as hard exudates. We do not deal with distinguishing optic disc from noisy parts or hard exudates. Instead we assign 0.5 to a channel having multiple ODs. It is possible that the OD can be detected at different positions at different channels for a retinal image. Reasons also could be the effect of noise or pathology. We keep this issue to be solved for future. The OD based score for a retinal image can be in the range $0 - 4$. Unlike other score estimation steps, we do not use the FGM in this step. The size of OD, to some extent depends on ethnicity. Therefore, if the ethnic group in the test set is different from the ethnic group of our development set (i.e., UoA_DR), then our approach might fail to detect OD

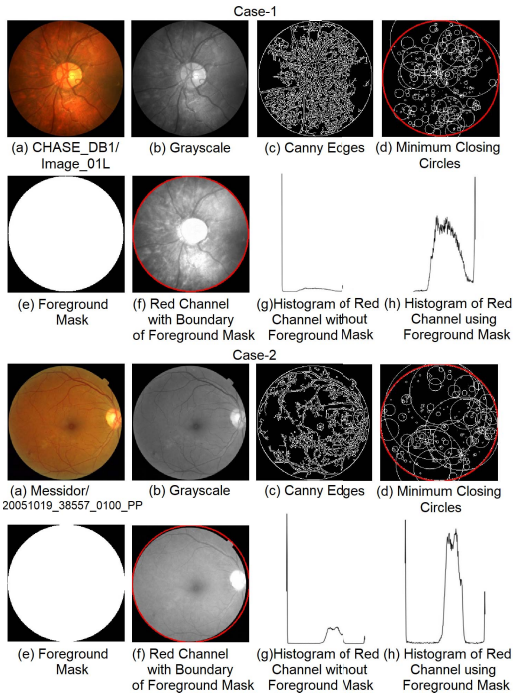

Fig. 4. Steps for generating FGM and the effect of FGM on the histogram.

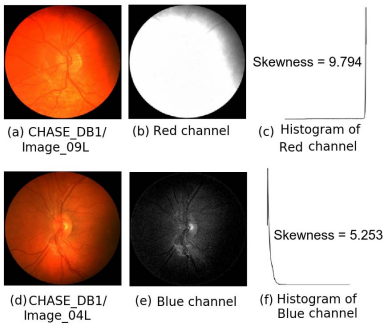

Fig. 5. Histograms of overexposed and underexposed channels.

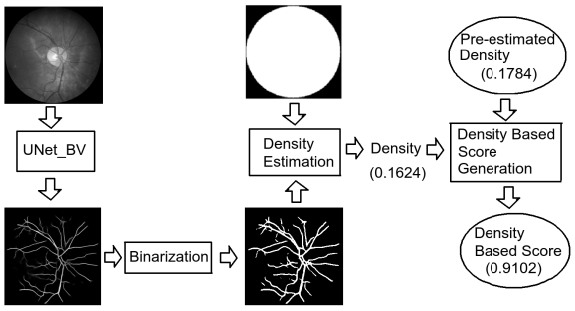

Fig. 6. Steps for the density of CRBVs based score estimation.

and give mistakenly lower quality score to a retinal image.

IV. Results & Analysis

In this paper, the evaluation of our approach is limited to inspection and analysis of a subset of the graded images. A quantitative evaluation will be performed in future. In total we estimate quality scores of 3090 images. We categorize images into three categories (i.e., *poor*, *fair* and *good*) by drawing two lines between the highest score (i.e., 15.32) and the lowest score (i.e., 6.032). Fig. 7 shows some sample images of these three categories. Both the highest and lowest scores are from the Kaggle_SetA data set. Fig. 8 and Fig. 9, show how the worst scorer and the best scorer get scores. Among 3090 images, 1854 images (i.e., 60%) fall into the *good category*, whereas 1158 images (i.e., 37.5%) into the *fair category* and 27 images (i.e., 2.5%) into the *poor category*. As shown in Fig. 10, there is no image of the CHASE_DB1 data set in the poor category.

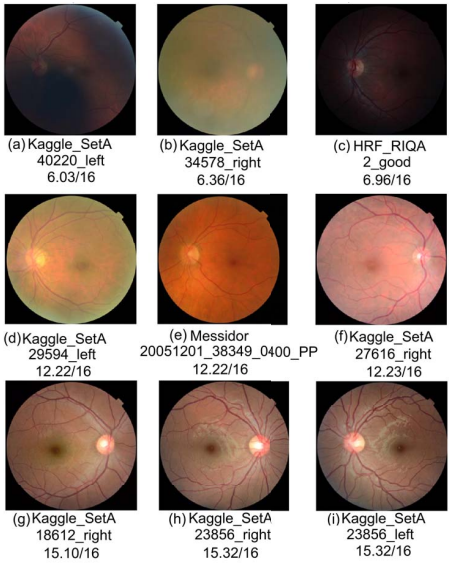

Fig. 7. Three sample images from the good, fair and poor categories. 1st row: poor category, 2nd row: fair category, 3rd row: good category. On the caption of each image database name, image file name, and quality score estimated by our approach are shown.

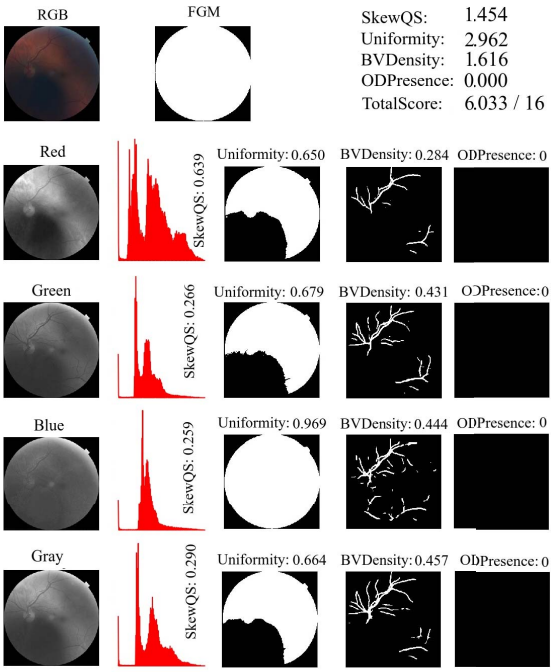

Fig. 8. Score analysis of the image (i.e., Kaggle_SetA/40220_left) having the worst score.

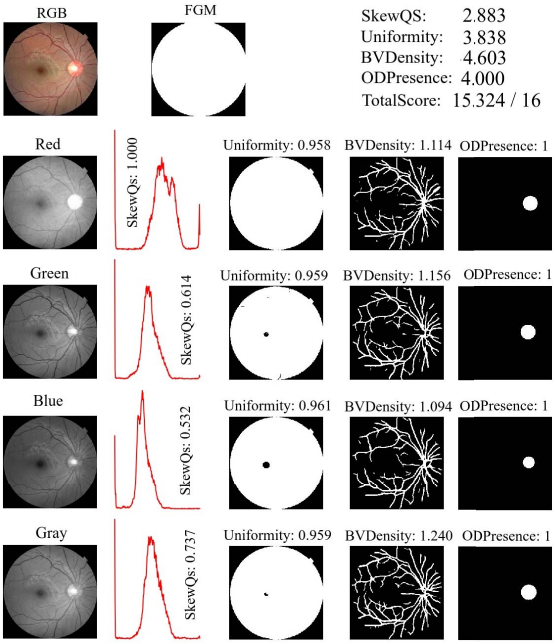

Fig. 9. Score analysis of the image (i.e., Kaggle_SetA/23856_right) having the best score.

To load and resize a retinal image, generate scores by analyzing 4 features for each channel and save the result, it takes on average 3.2 seconds on our GPU based system. On the other hand, in an Intel(R) Core(TM) i5-7500 CPU based machine these tasks take on average 6.91 seconds.

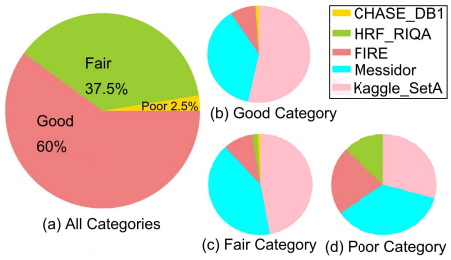

Fig. 10. Category wise pie charts.

There are some limitations of our current approach. Our approach is not a pure *non-reference* based approach. Therefore, it would suffer from the mismatch of the development set and the test set. The effect of the camera lens flare problem has not been dealt with.

V. Conclusion

Since poor quality retinal images not only increase the possibility of wrong diagnosis or incorrect person recognition but also increase the diagnosing or recognition time, Retinal Image Quality Assessment (RIQA) has become an important research topic. In this paper, we propose a RIQA approach by combining generic and content-based quality assessment approaches. We estimate quality of a retinal image by analyzing its histogram of pixel intensity, whether it is uniformly illuminated, as well as checking the presence of its two main anatomical structures, optic disc and central retinal blood vessels, in all color channels. By generating quality scores for five publicly available data sets, we show how our approach can help the fundus camera operators to assess quality.

Acknowledgement

This work was supported by The Ministry of Education, Youth and Sports of the Czech Republic from the National Programme of Sustainability (NPU II); project IT4Innovations excellence in science - LQ1602.

References

[1] L. Abdel-Hamid, A. El-Rafei, S. El-Ramly, G. Michelson, and J. Hornegger. Retinal image quality assessment based on clarity and content. *SPIE JBO*, 21(9):096007–1–17, 2016.

[2] W. Abdulla and R. J. Chalakkal. University of Auckland Diabetic Retinopathy (UoA-DR) Database- END USER LICENCE AGREEMENT, 2018.

[3] M. D. Abràmoff, M. K. Garvin, and M. Sonka. Retinal imaging and image analysis. *IEEE Reviews in Biomedical Engineering*, 3:169–208, 2010.

[4] H. Bartling, P. Wanger, and L. Martin. Automated quality evaluation of digital fundus photographs. *Acta Opthalmologica*, 87:643–647, 2009.

[5] A. Budai, R. Bock, A. Maier, J. Hornegger, and G. Michelson. Robust Vessel Segmentation in Fundus Images. *Hindawi IJBI*, 2013.

[6] P. Costa, A. Campilho, B. Hooi, A. Smailagic, K. Kitani, S. Liu, C. Faloutsos, and A. Galdran. EyeQual: Accurate, Explainable, Retinal Image Quality Assessment. In *IEEE ICMLA*, pages 223–230, 2017.

[7] U. Şevik, C. Ḱose, T. Berber, and H. Erdöl. Identification of suitable fundus images using automated quality assessment methods. *Biomedical Optics*, 19(4):046006, 2014.

[8] J. Cuadros and G. Bresnick. EyePACS: An Adaptable Telemedicine System for Diabetic Retinopathy Screening. *SAGE JDST*, 3(3):509–516, 2009.

[9] E. Decencière, X. Zhang, G. Cazuguel, B. Lay, B. Cochener, C. Trone, P. Gain, R. Ordonez, P. Massin, A. Erginay, B. Charton, and J.-C. Klein. Feedback on a publicly distributed database: the Messidor database. *Image Analysis & Stereology*, 33(3):231–234, 2014.

[10] A. D. Fleming, S. Philip, K. A. Goatman, J. A. Olson, and P. F. Sharp. Automated Assessment of Diabetic Retinal Image Quality Based on Clarity and Field Definition. *ARVO IOVS*, 47(3):1120–1125, 2006.

[11] L. Gagnon, M. Lalonde, M. Beaulieu, and M.-C. Boucher. Procedure to detect anatomical structures in optical fundus images. In *Medical Imaging*, volume 4322, pages 1218–1225, 2001.

[12] L. Giancardo, F. Meriaudeau, T. P Karnowski, E. Chaum, and K. Tobin. Quality Assessment of Retinal Fundus Images using Elliptical Local Vessel Density. In Domenico Campolo, editor, *New Developments in Biomedical Engineering*, chapter 11. IntechOpen, Rijeka, 2010.

[13] C. Hernandez-Matas, X. Zabulis, A. Triantafyllou, P. Anyfanti, S. Douma, and A. A. Argyros. Fire: Fundus Image Registration Dataset. *Journal for Modeling in Ophthalmology*, 1(4):16–28, 2007.

[14] A. Hoover, V. Kouznetsova, and M. Goldbaum. Locating Blood Vessels in Retinal Images by Piece-wise Threshold Probing of a Matched Filter Response. *IEEE TMI*, 19(3):203–210, 2000.

[15] Q. Huanga, W. Gaoa, and W. Caib. A Computational Approach to Edge Detection. *IEEE TPAMI*, PAMI-8(6):679–698, 1986.

[16] Q. Huanga, W. Gaoa, and W. Caib. Thresholding technique with adaptive window selection for uneven lighting image. *Elsevier PRL*, 6:801–808, 2005.

[17] T. Köhler, A. Budai, M. F. Kraus, J. Odstrčilik, G. Michelson, and J. Hornegger. Automatic no-reference quality assessment for retinal fundus images using vessel segmentation. In *IEEE CBMS*, pages 95–100, 2013.

[18] M. Lalonde, L. Gagnon, and M. Boucher. Automatic visual quality assessment in optical fundus images. In *Proceedings of Vision Interface*, pages 259–264, 2001.

[19] S. C. Lee and Y. Wang. Automatic retinal image quality assessment and enhancement. In Kenneth M. Hanson, editor, *Medical Imaging 1999: Image Processing*, volume 3661, pages 1581 – 1590. International Society for Optics and Photonics, SPIE, 1999.

[20] S. C. Nemeth, C. Shea, M. DiSclafani, and M. Schluter. *The Posterior Segment*, chapter 9, pages 88–99. Slack Incorporated, Thorofare, NJ, USA, 2 edition, 2008.

[21] M. Niemeijer, Michael D. Abràmoff, and Bramvan Ginnekena. Image structure clustering for image quality verification of color retina images in diabetic retinopathy screening. *Medical Image Analysis*, 10:888–898, 2006.

[22] S. R. Nirmala, S. Dandapat, and P. K. Bora. Wavelet weighted blood vessel distortion measure for retinal images. *Elsevier BSPC*, 5:282–291, 2010.

[23] N. Otsu. A threshold selection method from gray-level histograms. *IEEE TSMC*, 9:62–66, 1979.

[24] C. G. Owen, A. R. Rudnicka, R. Mullen, S. A. Barman, D. Monekosso, P. H. Whincup, J. Ng, and C. Paterson. Measuring Retinal Vessel Tortuosity in 10-Year-Old Children: Validation of the Computer-Assisted Image Analysis of the Retina (CAIAR) program. *IOVS*, 50:2004–2010, 2009.

[25] J. Paulus, J. Meier, R. Bock, J. Hornegger, and G. Michelson. Automated quality assessment of retinal fundus photos. *Springer IJCARS*, 5:557–564, 2010.

[26] R. Pires, H. F. Jelinek, J. Wainer, and A. Rocha. Retinal Image Quality Analysis for Automatic Diabetic Retinopathy Detection. In *SIBGRAPI*, pages 229–236, 2012.

[27] O. Ronneberger, P. Fischer, and T. Brox. U-net: Convolutional Networks for Biomedical Image Segmentation. *MICCAI*, 9351:234–241, 2015.

[28] S. K. Saha, B. Fernando, J. Cuadros, D. Xiao, and Y. Kanagasingam. Automated Quality Assessment of Colour Fundus Images for Diabetic Retinopathy Screening in Telemedicine. *Springer JDI*, 31:869–878, 2018.

[29] J. J. Staal, M. D. Abramoff, M. Niemeijer, M. A. Viergever, and B. van Ginneken. Ridge based vessel segmentation in color images of the retina. *IEEE TMI*, 23(4):501–509, 2004.

[30] H. Yu, C. Agurto, S. Barriga, S. C. Nemeth, P. Soliz, and G. Zamora. Automated image quality evaluation of retinal fundus photographs in diabetic retinopathy screening. In *IEEE SSIAI*, pages 125–128, 2012.

[31] G. T. Zago, R. V. Andre ao, and B. Dorizzi. Retinal image quality assessment using deep learning. *Computers in Biology and Medicine*, 103:64–70, 2018.